VIBRATION AND SOUND RADIATION OF A PIANO SOUNDBOARD

JUNE 18, 1984

By: Hideo Suzuki
CBS Technology Center
227 High Ridge Road
Stamford, CT

VIBRATION AND SOUND RADIATION OF A PIANO SOUNDBOARD

0 INTRODUCTION

A piano is a musical instrument which does not employ any acoustical resonator, even though it has a soundboard and strings as mechanical resonators. The soundboard is not an acoustical resonator, it is a direct radiator which converts mechanial energy into acoustical energy. Since a large sound output is required from very low frequencies, the piano soundboard must be very large, yet it must still be light. The wavelength of the sound corresponding to the lowest notes of the piano are still much larger than the size of the soundboard. In this range, the sound radiation may not be efficient due to the cancellation between the sound produced by the front and rear of the soundboard. For wavelengths corresponding to higher notes, the size of the soundboard becomes relatively large and the above mentioned cancellation may gradually disappear. In this frequency region, the soundboard does not vibrate as a piston, but vibrates with various mode shapes. Then, cancellation among different areas of the soundboard surface starts to take place.

This effect depends on the speed of sound in air and the speed of the flexural wave in the soundboard.

Since the structure and the shape of the soundboard are so complex, it is very difficult to theoretically investigate the vibration and radiation characteristics. Thus, the studies performed in the past have been mostly experimental. Even though researchers have studied the piano soundboard for many years, a good understanding of the soundboard has yet to be obtained. The following are some intesting problems in investigating the vibration and radiation characteristics of the piano soundboard:

(1) What are the frequencies and vibration patterns (modal shapes) of the fundamental resonances of the soundboard?

(2) What kind of relationship is observed between the vibration and the radiation patterns?

(3) Which areas on the soundboard contribute to the sound radiation?

(4) How much power is radiated per unit force applied on the bridge?

(5) How does the radiation efficiency change as a function of frequency?

In the present paper, the vibration and radiation characteristics of the piano soundboard (supported by a rim without strings) will be investigated, keeping these problems in mind.

A commonly used technique to measure the vibration patterns of the soundboard is the Chladni method. This technique is very simple in its application, but it does not provide quantitative results. Instead, the recently developed modal analysis method [1-3] is used for the investigation of the vibration characteristics.

Three methods are considered in measuring sound intensity. Those are: (1) surface intensity method [4-6], (2) two-microphone method [7-9],and (3) acoustical holography [10-11]. In the surface intensity method, the sound intensity normal to a surface is calculated from the velocity and pressure information on the surface. Since the velocity is always necessary for the modal analysis of the vibration characteristics, the intensity information is simply obtained by an additional measurement of the sound pressure distribution. This method, therefore, seems appropriate considering the geometry of the soundboard and the purpose of the study.

I. MEASUREMENT

1.1 Measurement Setup

The block diagram of the measuring system is shown in Fig. 1. A Dynamic Structural Analyzer (Hewlett-Packard, 5423A) was used to control the measurement system. This analyzer is designed for the modal analysis of a structure in general. A noise signal from the analyzer is fed to a shaker (MB Electronics, model EA1500) which is connected to the soundboard by a 0.5" diameter brass rod with a force trandsucer (PCB, model 200B) at the end of the rod. The force transducer measures the excitation force applied to the soundboard by the shaker. This signal is used as the input to channel 1 of the analyzer. At the same time, an accelerometer (PCB, model 309A) picks up the acceleration at a point on the soundboard. This signal is used as the input to the channel 2. The analyzer calculates the transfer function $H^a(\omega)$ between two signals and stores it on a data tape. Then, channel 2 is switched to the pressure signal from a microphone located at the same point as the acceleration measurement. Again, the transfer function $H^p(\omega)$ is calculated and stored on the data tape next to $H^a(\omega)$. The same process is repeated for different locations on the sound board giving

$H^a_{m,n}(\omega)$ and $HP_{m,n}(\omega)$ where m and n indicate the driving and receiving points, respectively. The driving point m was fixed and the receiving point n was varied from 1 to 150 covering the entire soundboard.

1.2 Modal Analysis

Since the modal analysis method is fairly common, this method will be outlined only briefly. The first step is to assign mode numbers to the resonances which are observed as peaks of the transfer functions $H^a_{m,n}(\omega)$. Then, by choosing a representative transfer function, the frequency and damping of each mode are calculated using a curve fitting algorithm. Once the representative frequencies and dampings are given for individual resonances, the relative amplitude v_n (including phase information) of each mode at every point n is calculated again using a curve fitting algorithm. This vector $\{v_n\}$ is called a mode shape. This mode shape can be graphically animated if the coordinates of the measurement points and the display sequence are given. If necessary, the modal mass and the stiffness for each mode can also be calculated. The animated

display of the vibration pattern is very helpful to better understand the characteristics of the modal vibrations.

1.3 Surface Intensity Method

The time-averaged intensity radiated from a vibrating surface is calculated as a function of frequency by

$$i = R_e \{p\ v^*\}/2, \qquad (1)$$

where the symbols R_e and * indicate the real part and the complex conjugate of a complex number, respectively; and p and v are the pressure and the normal velocity at the measurement point, respectively. So that we can calculate the intensity distribution and some other intensity-related quantities, the data stored on the data tape was sent to a VAX 11/780 host computer through an IBM PC. For the animated display of the radiation pattern, the intensity distribution calculated in the VAX 11/780 was sent back to the HP-5423A. When the vibration and the radiation patterns are compared, the following should be kept in mind. The radiation pattern is the intensity distribution when the soundboard is driven at a specific point and frequency.

The forced vibration of the soundboard in this case contains all the modes even though the mode(s) closest to the driving frequency is dominant. On the other hand, the vibration pattern (mode shape) is a pattern of a specific mode which is irrelevant to the driving point and frequency.

The major drawback of the surface intensity method is the difficulty in the phase calibration between the accelerometer and the pressure microphone. In the low-frequency range where the radiation efficiency is small, the pressure and the velocity are almost 90° out-of-phase (which is called a "reactive field"), and a small error of the phase measurement results in a significant error in the intensity calculation. Therefore, the phase mismatch between the two transducers must be calibrated as accurately as possible. This was accomplished by using the calibration device shown in Fig. 2. The calibrator consists of a body with a small air chamber and a driver. When the driver is excited by a shaker, the sound pressure inside the chamber is 180° out-of-phase with the acceleration of the driver. Thus, by putting the accelerometer on the driver and facing the microphone onto the air chamber, the difference of the phase responses ($\phi_a - \phi_p$) is measured, where ϕ_a and ϕ_p are the phase responses of the accelerometer and the microphone. The result is shown in

Fig. 3. The phase difference is almost zero around 200 Hz, but it is significantly large in the low-frequency region. At 50 Hz, for example, the phase difference is about -10°. This phase response was also sent to the VAX 11/780 and used for calibration when the intensity was calculated using Eq. (1). In Section 2.4, two results, one with calibration and the other without, will be compared to see the effect of the calibration on the accuracy of the measurement.

1.4 Test Soundboard and Measurement Points

The shape and dimensions of a test soundboard of a six-foot grand piano are shown in Fig. 4. The measurement was performed on a soundboard with a rim and a brace, but without a cast-iron plate and strings. The soundboard has a thickness of approximately 0.25-0.3 inches. Figure 4 also shows by a dot the point of excitation (Point 76) and the 150 measurement points (intersection of lines). The excitation point is the point on the bridge corresponding to the note C4# (key number 41).

II. RESULTS AND DISCUSSION

2.1 Comparison of $H^a(\omega)$ and $H^p(\omega)$

It was expected that the comparison of $H^a(\omega)$ and $H^p(\omega)$ would show a qualitative difference between the vibration and radiation characteristics. For this reason, the transfer functions $H^a(\omega)$ and $H^p(\omega)$ were plotted at a rate of one for every five points. Figure 5 shows these results. The left and right columns are for $H^a(\omega)$ and $H^p(\omega)$; and the top, middle, and bottom charts are for the points from 1 to 46, 51 to 96, and 101 to 146, respectively. The $H^a(\omega)$ function has larger variations as a function of position than $H^p(\omega)$ does even though the peaks of the two kinds of transfer functions correspond well to each other. The reason for the large deviation of $H^a(\omega)$ is due to the fact that the vibrations along the edge are quite small except at the resonance frequencies of the rim. Meanwhile, the sound tends to propagate on the the entire surface making the distribution more uniform.

The other difference between $H^a(\omega)$ and $H^p(\omega)$ is the level change as a function of frequency. Relatively speaking, the level change of $H^a(\omega)$ is smaller than that of $H^p(\omega)$.

The latter decreases gradually as the frequency increases in the range from 50 Hz to 200 Hz. The numbers shown around the peaks of $H^a(\omega)$ in the middle left chart of Fig. 5 are the assigned mode numbers for the modal analysis. The mode shapes of these resonances will be discussed in the following section. (The numbers shown in the middle right chart of Fig. 5 will be explained in Section 2.3.)

2.2 Vibration Pattern

Once the representative frequency and damping are assigned to each mode, the analyzer can extract the amplitude information of the mode at every point using a curve fitting algorithm. The vibration patterns (mode shapes) obtained in this manner are shown in Figs. 6 - 12. from the 1st mode to the 7th mode.

The first vibration mode is very simple and similar to the vibration of a trampoline. The 2nd mode is the first break-up mode in the length direction. The two points near the top right corner of the soundboard are on the bass bridge and show larger amplitudes than the others (this is also true for the 3rd and 5th modes). The 3rd mode is very similar to the second mode except that the former has a large amplitude along the edge. Also, the amplitude of the lower center portion is larger than that of the

upper center portion for this mode. This mode may be considered as a superposition of the 2nd mode of the soundboard and the 1st bending mode of the rim. At most frequencies, the assumption of fixed support seems reasonable as the boundary condition for the soundboard. At rim resonances, however, this is not valid as the 3rd mode indicates. It seems important to discriminate between these two modes (2nd and 3rd modes) clearly when investigating the soundboard, since the frequency of the rim resonance may be affected by the support condition of the whole system. The 4th mode is the first break-up mode in the width direction. (This may be considered as the 3rd resonance of the soundboard itself.) The 5th mode is a pattern having two nodal lines in the length direction that are not parallel to the keyboard. The 6th mode shows four areas, the top left and bottom right vibrate in phase with each other and vibrate out of phase with the other two areas. The 7th mode is more complex and shows several nodal lines as well as a large amplitude along the edge showing the effect of another rim resonance.

The resonance frequency and the loss factor (abbreviated as LF in the figure) of each mode is shown at the lower right corner of its vibration pattern. The frequency of the 1st mode is 49.7 Hz, and that of the 7th mode is 195.44 Hz, having an average

spacing of about 25 Hz between adjacent modes. The dampings (or the loss factors) of the modes are very small. They are 0.064 for the first mode and approximately 0.02 - 0.03 for the higher modes. The loss factor of a spruce plank measured at our laboratory is approximately 0.013 - 0.016. The additional damping of the soundboard may be due to the radiation resistance and the structural damping.

2.3 Radiation Pattern

The accuracy of the surface intensity method depends on the accuracy of the phase calibration of the transducers and the phase difference between the velocity and the sound pressure on the surface. If the sound field is highly reactive, the accuracy of the measurement decreases. If the sound radiation is more efficient, a more accurate measured result is available for a given phase calibration. In Section 2.5, the degree of radiation efficiency will be discussed in terms of the normalized radiation resistance. For the analysis of the radiation pattern, six frequency points were chosen at which the radiation efficiency was large enough to ensure the accuracy of the intensity calculation. These points are indicated by numbered arrows in the middle right chart in Fig. 5. The radiation patterns at these frequencies are shown in Figs. 13-18.

The radiation pattern at 107 Hz (Fig. 13) shows a large intensity region on the left side of the soundboard. This pattern is more or less like a superposition of the 3rd and 4th vibrational modes (Figs. 8 and 9) except that the right top corner of the soundboard does not have large negative intensity. In the second and third radiation patterns (Figs. 14 and 15), the area of the largest intensity is the lower middle part and right side of the soundboard, respectively. Since the frequencies of these three radiation patterns are between modal frequencies, some area may have a small velocity amplitude when the two adjacent modes are superimposed. This might be the reason the radiation area with large intensity is restricted to a narrower region than imagined from the modal vibration patterns. From the 4th radiation pattern at 168 Hz, the radiation area seems to become wider than for the previous radiation patterns. These radiation patterns at higher frequencies have a very small area with negative intensity indicating that the radiation efficiency is greater in this range. It is interesting that the intensity at the driving point is not necessarily positive. It is expected that the sound energy absorbed into one area of the soundboard is partly consumed as a mechanical loss and partly transmitted from other areas of the soundboard.

2.4 Power Response and Radiation Efficiency

The total radiated power W is obtained by integrating the intensity on the surface of the soundboard (upper side only) such as:

$$W = \int I ds \qquad (2)$$

The results are shown in Fig. 19. Below 90 Hz, the radiated power is small except around the peak at 50 Hz. This indicates that the sound field is very reactive (i.e., the phase difference between the velocity and the pressure is close to 90 degrees). As mentioned earlier, it is safe to assume that the present intensity measurement is accurate enough above 90-100 Hz. The radiated power characteristics, when the bridge is driven by a constant force (1 dyne), has peaks at the frequencies corresponding to the resonances of the soundboard. In a practical situation when the bridge is driven by strings, it can be said that a larger amount of energy is radiated when the string resonances are closer to the soundboard resonances, resulting in a quick decay to the corresponding harmonics.

Figure 20 shows the same result on a decibel scale normalized to 10^{-6} watt. In the frequency range where the power becomes negative, it was replaced by a small positive value and then a logarithm was taken. The characteristic is similar to the pressure characteristics shown in Fig. 5 (P2). The fluctuation of the radiated power is within ∓5 dB in the range from 100 Hz to 210 Hz. This seems relatively small considering the fluctuation of the vibration characteristics in the same range.

A normalization of the radiated power to the input power gives the radiation efficiency, which is defined as:

$$\eta = W/[R_e(F_d v_d^*)/2.0] \qquad (3)$$

where F_d is the force applied at the driving point (1 dyne in the present case) and v_d is the resulting velocity at the same point. Figure 21 shows this result. It is interesting that there is no peak in the radiation efficiency corresponding to the large peak of the radiated power at 50 Hz in Fig. 19. Above 90 Hz, the radiation efficiency averages roughly 15%. It can be said that the mechanical energy of a string is converted into sound energy with the efficiency of approximately 30% in this

range assuming that the same amount of energy is radiated from the lower side of the soundboard. The soundboard of a six-foot grand piano seems to be a fairly efficient mechano-acoustical transducer above 90 Hz.

2.5 Normalized Radiation Resistance

Another way of looking at the radiation characteristic is the normalized radiation impedance. The normalized radiation impedance of a radiator having a uniform velocity V and an area S is calculated by:

$$z = W/\rho cS \left|V\right|^2, \qquad (4)$$

where W is the radiated power, (which is complex including the reactive power), and ρc is the characteristic impedance of air. For a radiator with a non-uniform velocity distribution v, the normalized radiation impedance can be defined in a similar manner such as:

$$z = W/\int \rho c \left|v\right|^2 dS \qquad (5)$$

The normalized radiation resistance (real part of Eq. (5)) was calculated as a function of frequency. The result is shown in Fig. 22. Curve (a) is the radiation resistance when the phase error is calibrated using the response shown in Fig. 3. For comparison, the resistance characteristic without calibration is also shown as curve (b) in the same figure. Without phase calibration, the resistance becomes mostly negative below 80 Hz, indicating the inaccuracy of the measurement. With the phase calibration, the resistance curve approaches zero as the frequency decreases. This seems reasonable for a soundboard which has the property of a quadrapole or a dipole at very low frequencies. Fig. 22 indicates that the measurement is accurate above 100 Hz except for a couple of frequencies where the radiation resistance becomes very small. Those frequencies are 116 Hz and 136 Hz which correspond exactly to the resonance frequencies of the 4th and 5th vibrational modes. This is why these frequencies were avoided when observing the radiation pattern.

Below 90 Hz, the normalized radiation resistance is very small. The low radiation efficiency below 90 Hz seems to be due to the cancellation between the sound radiated from the upper

and lower surfaces of the soundboard . Above this frequency, the distance between the upper and lower radiating surfaces becomes equal to or larger than the half wavelength of sound and, therefore, the dipole effect ceases to play a major role.

In the range from 90 Hz to 210 Hz, the normalized radiation resistance is highly frequency dependent. Since the bending wavelength of the soundboard is still shorter than the wavelength of sound in air, the cancellation of sound among different areas of the soundboard is possible if they vibrate out-of-phase. This is confirmed by calculating the normalized volume velocity, β , defined as:

$$\beta = \left| \int v dS \right| / \int |v| dS \qquad (6)$$

where the normalization is necessary to remove the effect of the mechanical resonance. The normalized volume velocity is equal to unity if the soundboard vibrates in-phase over the entire surface. The characteristic of this volume velocity is shown in Fig. 23. Above 90 Hz, a strong correlation between the normalized radiation resistance and the normalized volume velocity is observed, indicating that the volume velocity is a

major factor in determining the normalized radiation resistance in this frequency range. It is interesting that the volume velocity becomes very small at some of the soundboard resonances (2nd, 4th, and 5th modes). This might be the reason that a consistant sound output is observed even though sharp mechanical resonances cause large deviations in the vibration amplitude over the frequency range.

The normalized radiation resistance may approach unity as the frequency rises, since the bending wavelength is inversely proportional to the square root of frequency, whereas, the wavelength of sound in air is inversely proportional to the frequency. It is very interesting to find where the transition occurs from the inefficient (roughly speaking $z \leq 0.5$) to the efficient ($z \geq 0.5$) sound radiation.

III. CONCLUSION

In the low frequency region (10 Hz-210 Hz), the vibration and the radiation characteristics of a soundboard (with a rim and braces) used for a six-foot grand piano were studied. The vibration characteristics were analyzed using the modal analysis method, and the radiation characteristics were studied using the surface intensity method.

The soundboard used for the study shows seven major resonances below 210 Hz. The first (0,0) mode is at approximately 50 Hz, and its modal shape looks like a trampoline. The 2nd and 3rd modes are the first break-up modes in the length direction, that is, the (1,0) mode. The difference between them is that the 3rd mode is caused by a rim resonance. The 4th mode is the (0,1) mode showing one nodal line in the length direction. The (2,0), (1,1), (2,1) modes follow in this order. The average modal density is 1/25 Hz. The loss factors of the soundboard at the resonace frequencies are larger than the values obtained from a measurement of a spruce plank showing additional damping due to the air load.

The radiation pattern (intensity distribution) shows some similarity to the forced vibration pattern for the modes of lower order. Large differences are observed between the vibration and radiation patterns for modes of higher order. Generally speaking, the areas with negative intensity gradually decrease as the frequency rises.

The radiated power was calculated by integrating the intensity over the upper surface of the soundboard when the soundboard was driven by 1 dyne of force at a point on the bridge near the center. At the resonance frequencies of the soundboard, the radiated power becomes large. When it is normalized to the input power, however, the radiation efficiency is not necessarily large at the resonances. Above 90 Hz, the radiation efficiency is roughly 15% even though it is highly frequency dependent (one side only). Below 90 Hz, the radiation efficiency was too low for the present measurement system to evaluate the radiation characteristics in this region.

The normalized radiation resistance was calculated to evaluate the radiation efficiency in terms of the radiation impedance. Above 150 Hz, the normalized radiation resistance is

approximately 0.3. The radiation resistance is also highly frequency-dependent. The comparison of the radiation resistance to the volume velocity confirmed that the interaction among the sound radiated from different areas on the soundboard is the major cause of the large fluctuations in the radiation resistance.

What can we do to improve the radiation efficiency in the low frequency region? Since the low radiation efficiency below 90 Hz is caused by the cancellation of sound radiated from the upper and lower sides of the soundboard, this frequency can be lowered if the propagation path is made longer. For example, if the lower portion of the rim is made longer by 1-foot, the propagation path may increase approximately 1.5 feet. This lowers the frequency by approximately 20%. This would be a significant improvement. Above this frequency, the volume velocity (on one side of the soundboard) plays a major role in the radiation efficiency, which seems very difficult to control.

The present study was limited to a soundboard without strings and a plate. The addition of these two things may change the situation drastically. The next step will be to extend the measurement frequency range and to conduct measurements on a complete piano.

REFERENCES

[1] S.C. Walgrave and J.M. Ehlbeck, "Understanding Modal Analysis," SAE Paper No. 811046, October 1981.

[2] Structural Dynamics Research Corporation, MODAL-PLUS User Manual, August 1981.

[3] Hewlett-Packard, Modal Analyzer Manual (HP-5423A).

[4] J.D. Brito, "Machinery noise source analysis using surface intensity measurements," Noise-Con 79 Proceedings (1979).

[5] T. Hodgson, "Investigation of the surface acoustical intensity method for determining the noise sound power of a large machine in situ," J. Acoust. Soc. Am., 61, 487-493 (1977).

[6] M.C. McGary and M.J. Crocker, "Phase shift errors in the theory and practice of surface intensity measurements," J. Sound Vib., 82, 275-288 (1982).

[7] F.J. Fahy, "Measurement of acoustical intensity using the cross-spectral density of two microphone signals," J. Acoust. Soc. Am., 62, 1057-1059 (1977).

[8] H.P. Lambrick and W.A. Stahel, " A sound intensity meter and its application in car acoustics," Proceedings of Inter-Noise 1977, B142-B147 (1977).

[9] J.Y. Chung, J. Pope, and D.A. Feldmaier, "Application of acoustic intensity measurement to engine noise evaluation," Proceedings of the SAE Diesel Engine Noise Conference, Paper 790502, 33 (1979).

[10] E.G. Williams and J.D. Maynard, "Intensity vector field mapping with nearfield holography," Proceedings of INTER-NOISE 81, 1009-1012 (Netherlands 1981).

[11] P.R. Stepanishen and K.C. Benjamin, "Forward and backward projection of acoustic fields using FFT methods," J. Acoust. Soc. Am. 71, 803 (1982).

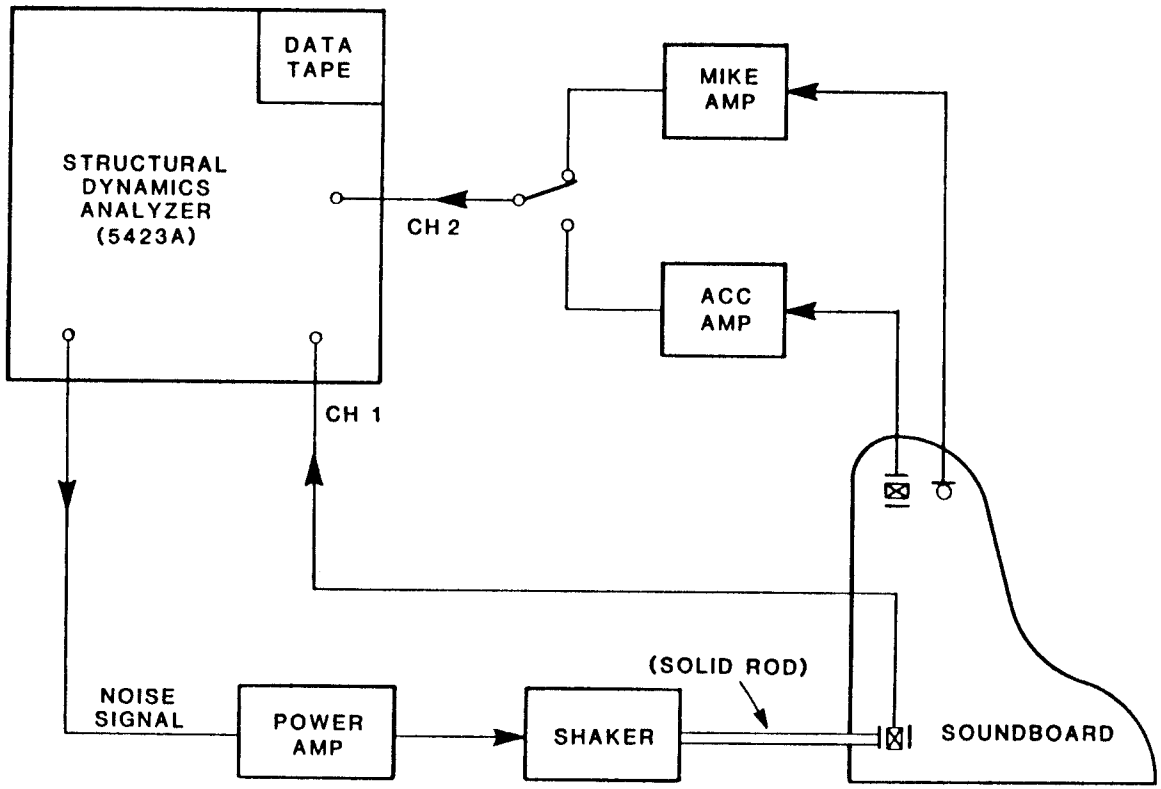

Fig.1 Measurement setup of the vibration and characteristics of a piano soundboard.

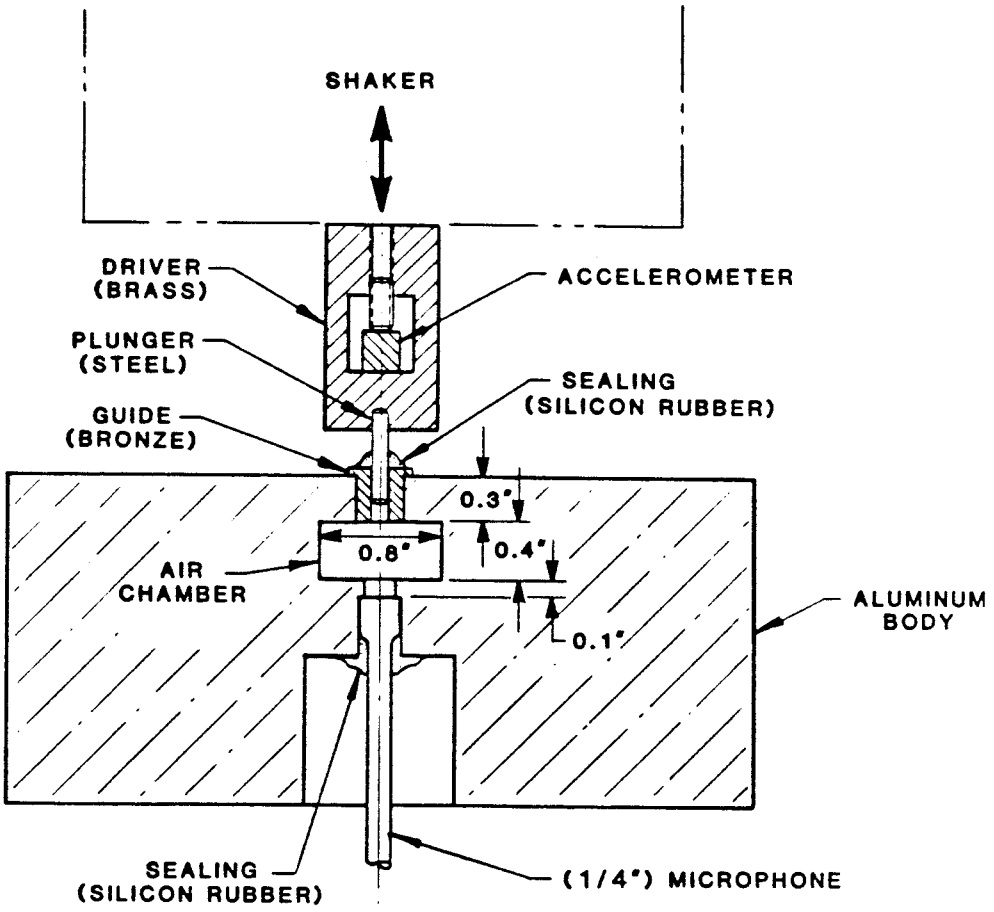

Fig. 2 Device used to calibrate the phase differences between the accelerometer and the microphone.

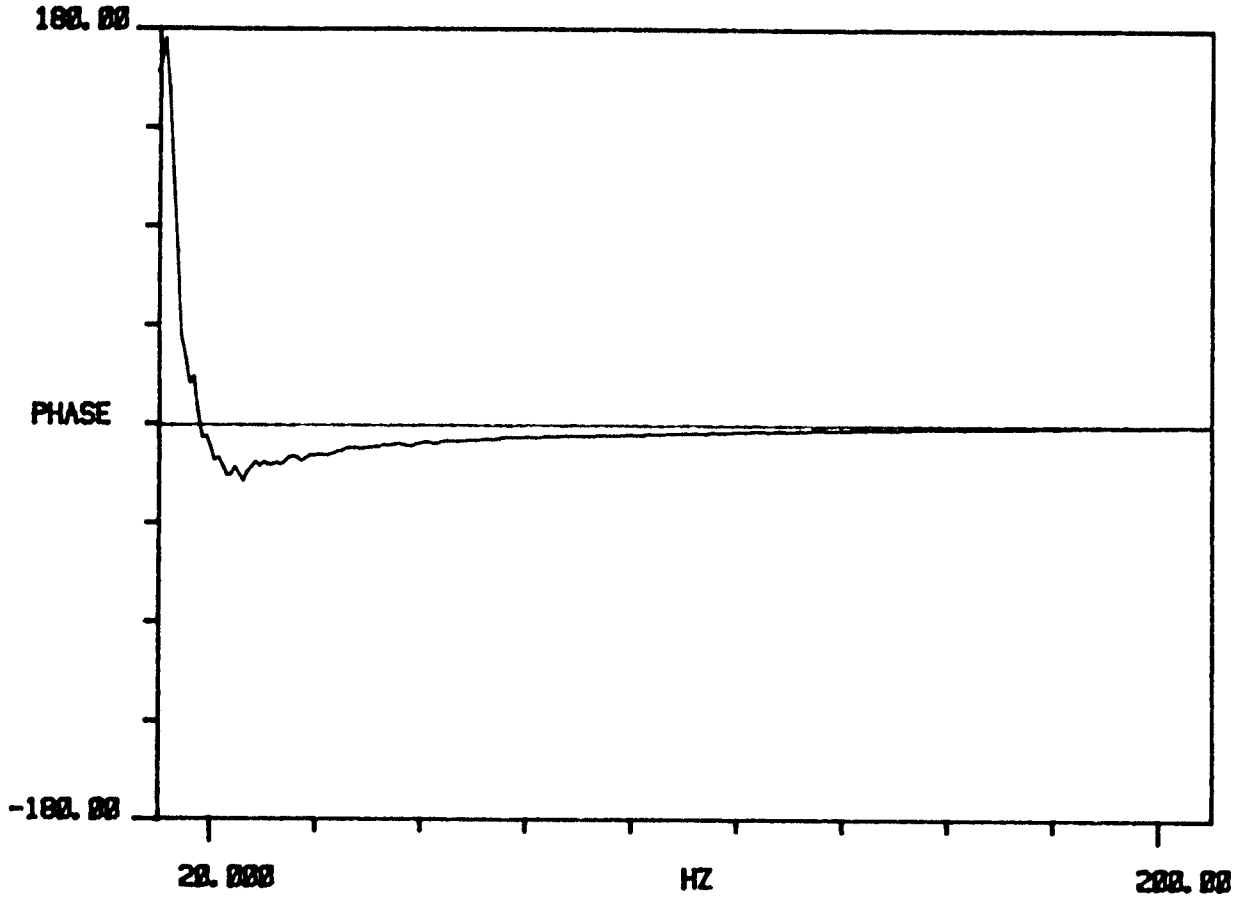

Fig. 3 Phase difference between the accelerometer and the microphone responses before calibration.

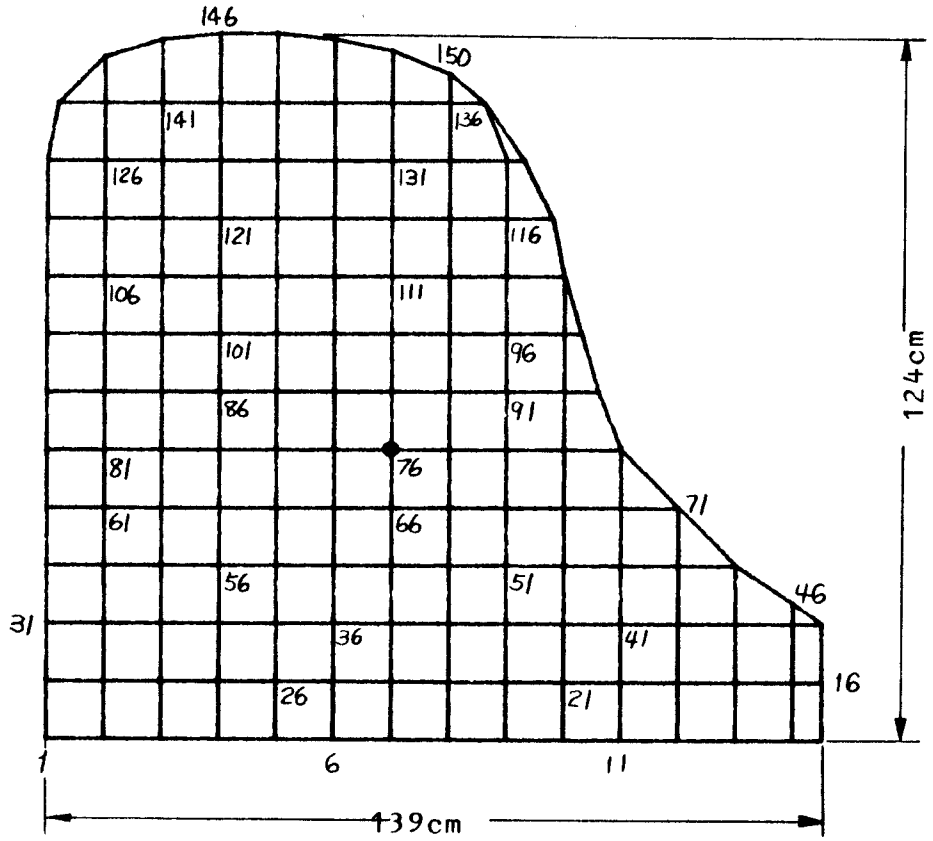

Fig. 4 Top view of the piano soundboard used for a six-foot grand piano. The acceleration and sound pressure were measured from Point 1 to Point 150 when the soundboard was excited at Point 76 on the bridge (shown by a dot).

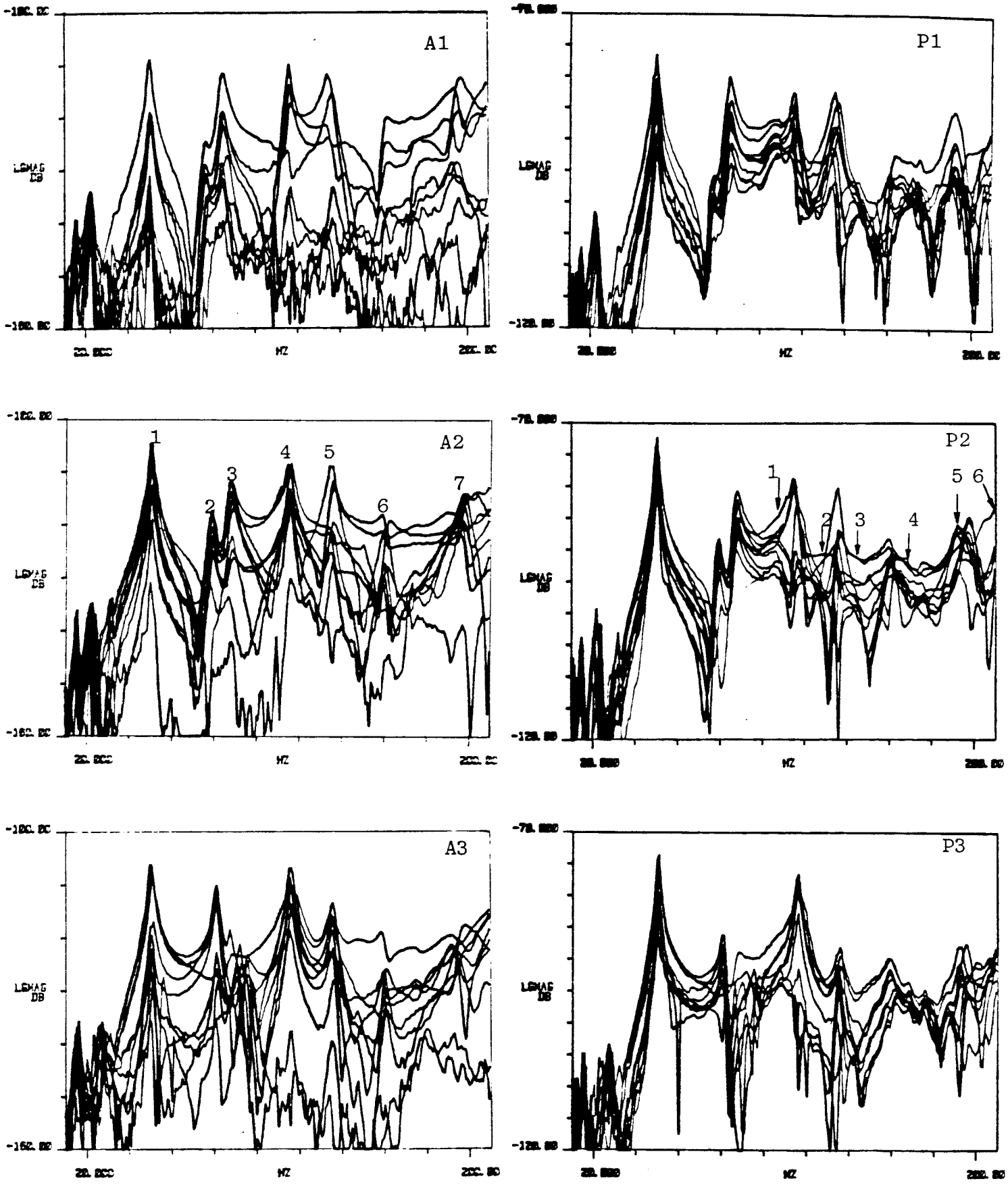

Fig. 5 Transfer functions $H^a(\omega)$ (A1-A3) and $H^P(\omega)$ (P1-P3). The top, middle, and bottom figures are for transfer functions between Point 76 (driving point) and 1, 6, ---, 46 (top), 51, 56, ---, 96 (middle), and 101, 106, ---, 146 (bottom), respectively.

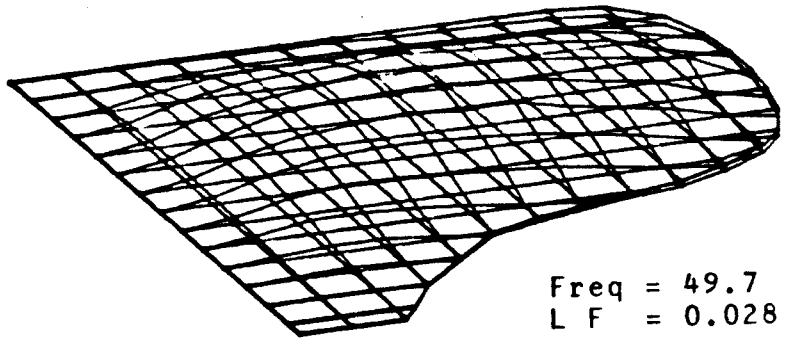

Fig. 6 Vibration pattern of the 1st mode.

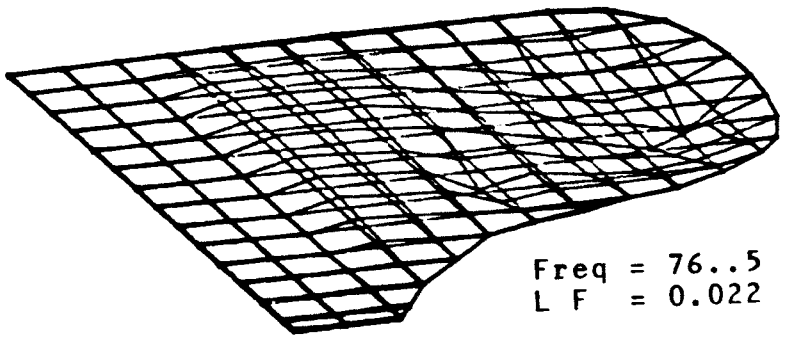

Fig. 7 Vibration pattern of the 2nd mode.

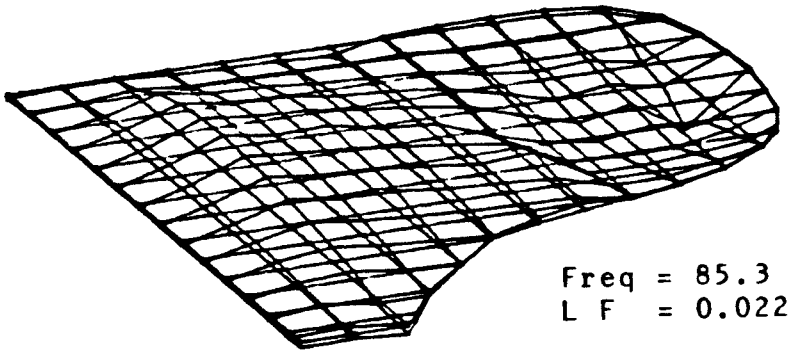

Fig. 8 Vibration pattern of the 3rd mode

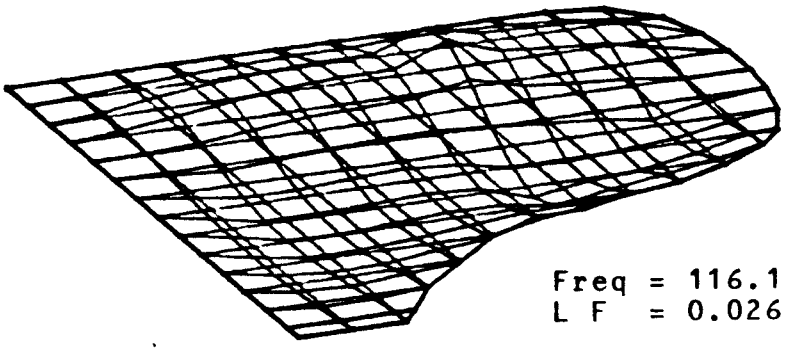

Fig. 9 Vibration pattern of the 4th mode

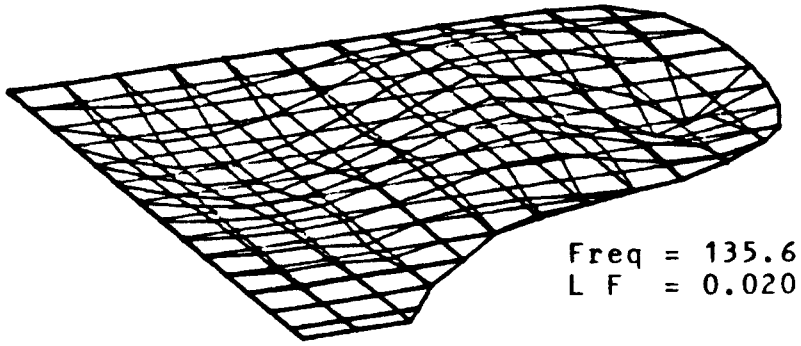

Fig. 10 Vibration pattern of the 5th mode

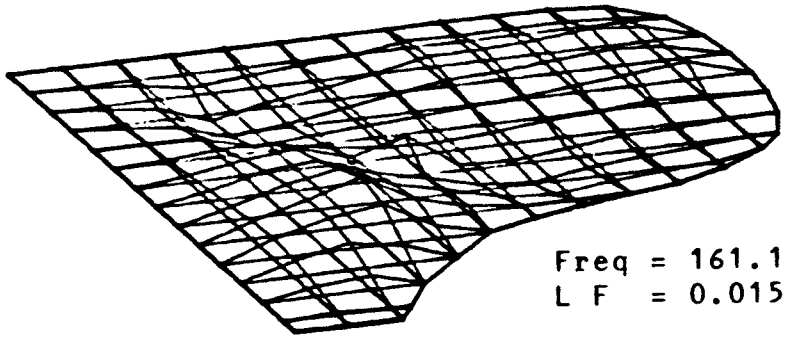

Fig. 11 Vibration pattern of the 6th mode

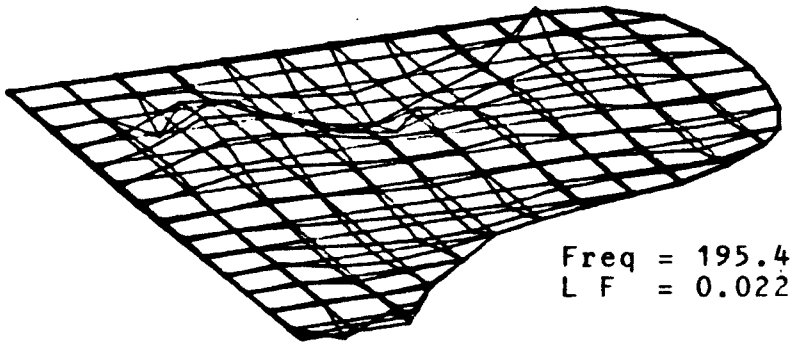

Fig. 12 Vibration pattern of the 7th mode

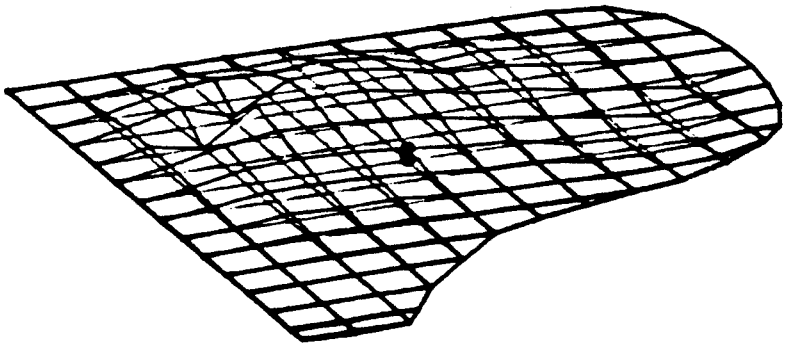

Fig. 13 Radiation pattern at 107 Hz (#1)

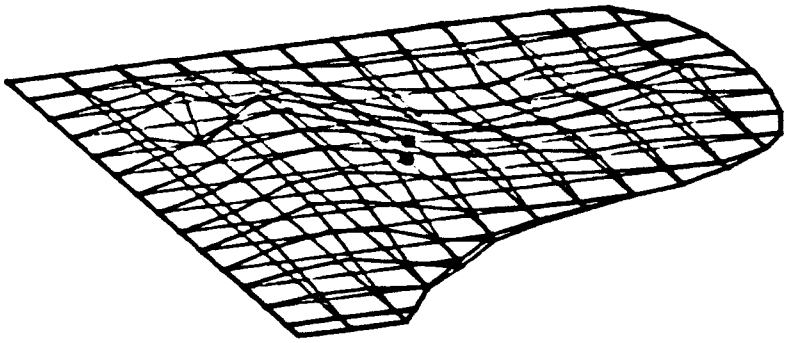

Fig. 14 Radiation pattern at 128 Hz (#2)

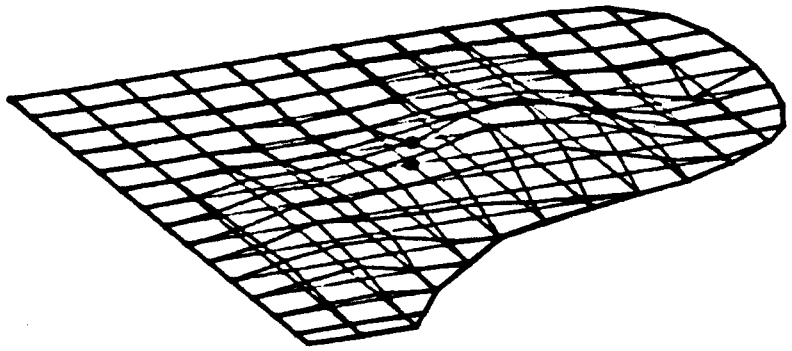

Fig. 15 Radiation pattern at 147 Hz (#3)

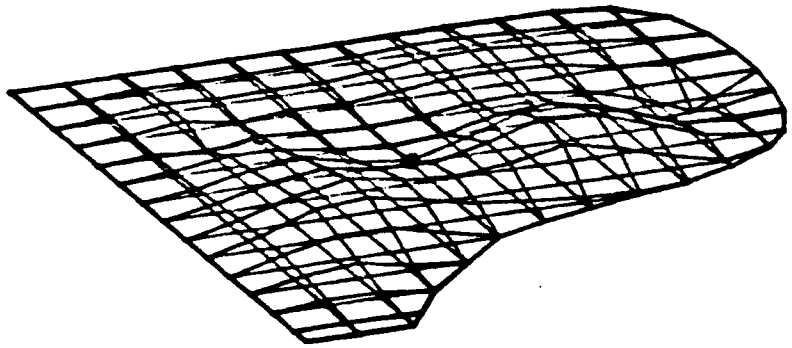

Fig. 16 Radiation pattern at 168 Hz (#4)

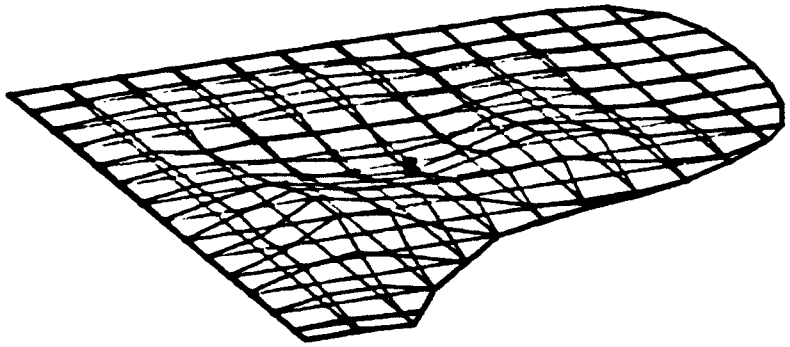

Fig. 17 Radiation pattern at 192 Hz (#5)

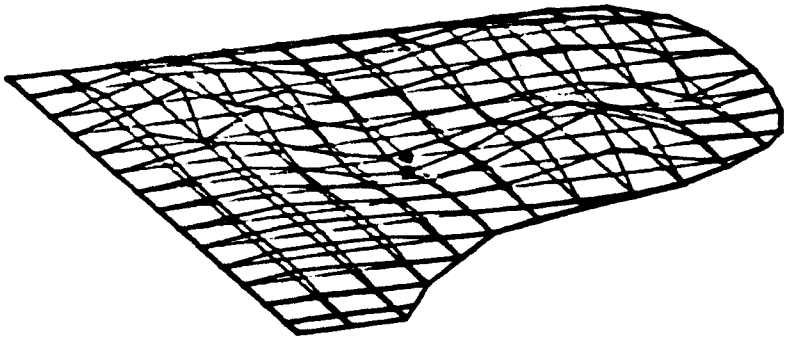

Fig. 18 Radiation pattern at 209 Hz (#6)

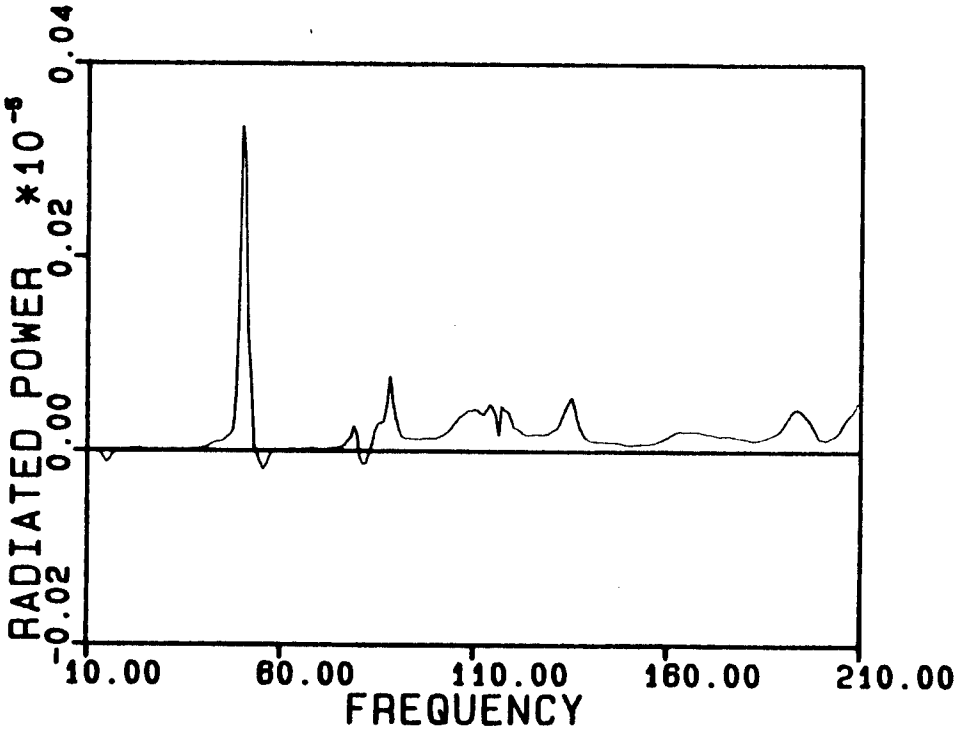

Fig. 19 Radiated power characteristic of the soundboard for a six-foot grand piano (linear scale).

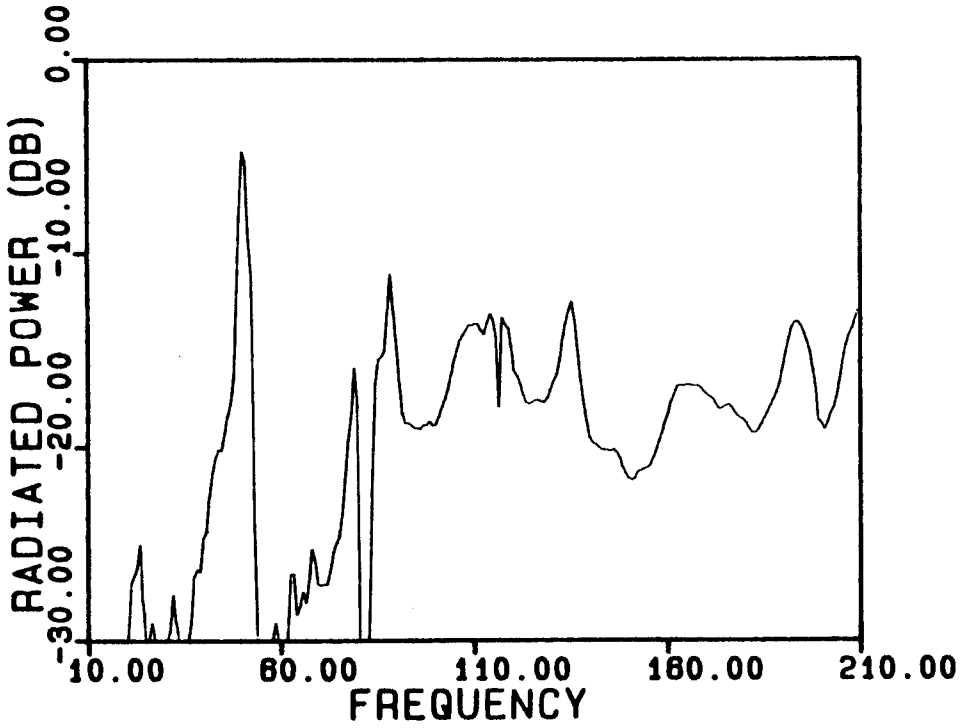

Fig. 20 Radiated power characteristic of the soundboard for a six-foot grand piano (dB scale).

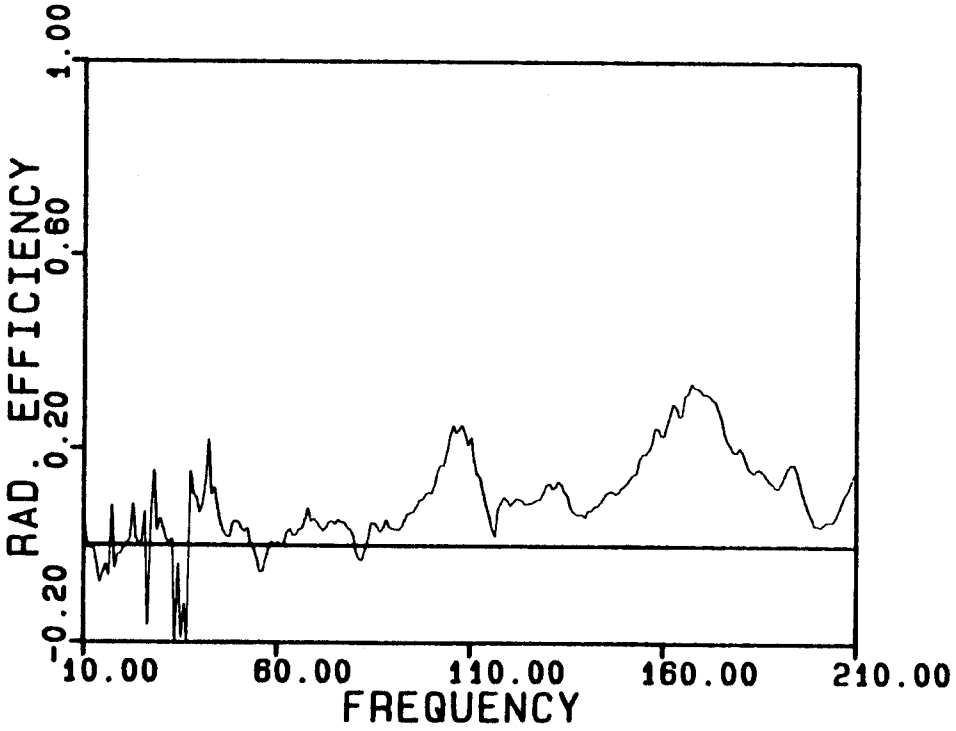

Fig. 21 Radiation efficiency characteristic of the soundboard for a six-foot grand piano.

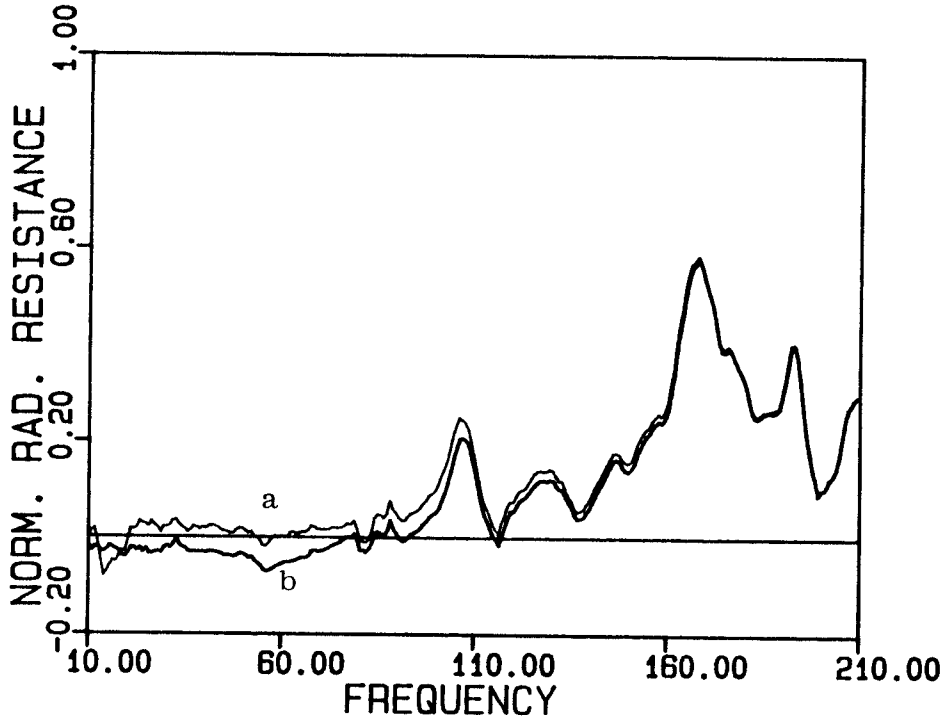

Fig. 22 Normalized radiation resistance characteristics with (a) and without (b) phase calibration.

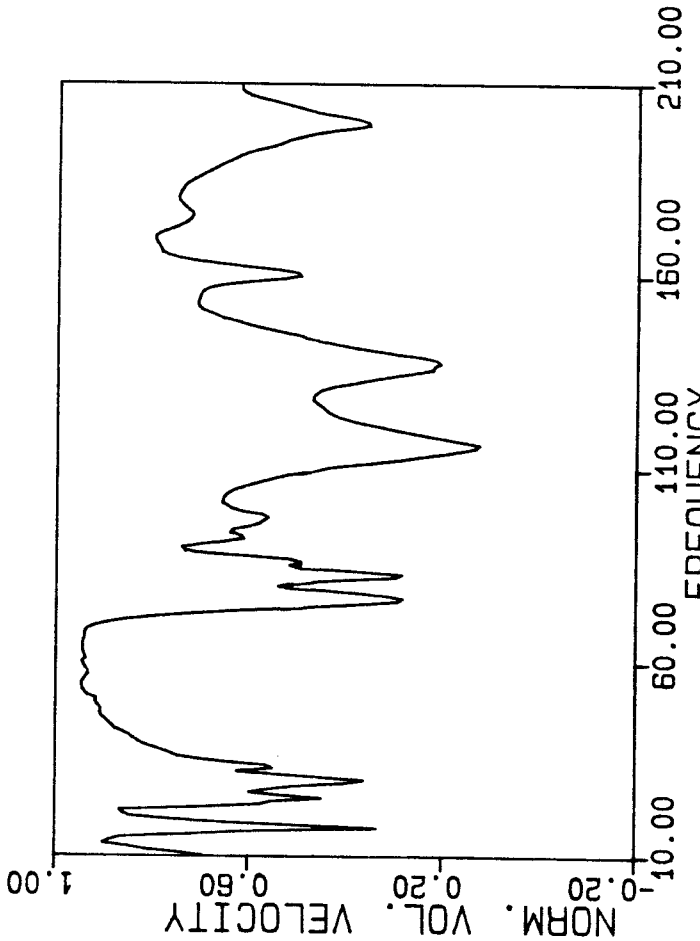

Fig. 23 Normalized volume velocity of the soundboard for a six-foot grand piano.